Title
ANGULAR DISTRIBUTION OF PROTONS FROM n- -p SCATTERING AT 900 Mev

Authors
Maglic, Bogdan C.
Feld, Bernard T.
Diffey, Carol A.

Publication Date
1961-02-01

UCRL-9594

UNIVERSITY OF CALIFORNIA

Ernest O. Lawrence Radiation Laboratory

BERKELEY, CALIFORNIA

DISCLAIMER

UNIVERSITY OF CALIFORNIA

Lawrence Radiation Laboratory
Berkeley, California

Contract No. W-7405-eng-48

ANGULAR DISTRIBUTION OF PROTONS FROM π^--p SCATTERING AT 900 Mev

Bogdan C. Maglić, Bernard T. Feld, and Carol A. Diffey

February 1961

ANGULAR DISTRIBUTION OF PROTONS FROM π^--p SCATTERING AT 900 Mev

Bogdan C. Maglić, Bernard T. Feld, and Carol A. Diffey
Physics Department and Laboratory for Nuclear Science
Massachusetts Institute of Technology

February 1961

ABSTRACT

The shape of the π^--p differential scattering cross section in the backward hemisphere should be sensitive to the nature of the "resonances" assumed to be responsible for the peaks in the total cross section at 600 and 900 Mev. The angular distribution of protons scattered in the forward hemisphere by pions of kinetic energy around 925 Mev, corresponding to pion c.m. angles from 65 deg to 150 deg, was obtained by placing nuclear emulsions close to liquid hydrogen and by measuring the direction angle and the grain count of every proton track.

It is shown that the sensitivity of emulsions in the temperature region $22^\circ K < T < 90^\circ K$ does not drop below 85% of the sensitivity at 300 $^\circ K$.

The resulting distribution is consistent with the assignment of $D_{3/2}^{1/2}$ and $F_{5/2}^{1/2}$ respectively, for the 600- and 900-Mev levels.

ANGULAR DISTRIBUTIONS OF PROTONS FROM π^--p SCATTERING AT 900 Mev

Bogdan C. Maglić,[†] Bernard T. Feld,[‡] and Carol A. Diffey

Physics Department and Laboratory for Nuclear Science
Massachusetts Institute of Technology

I. INTRODUCTION

Following the experiment by Frisch et al. on the π^--p cross section,[1] which first resolved the broad maximum near 900 Mev into two clearly separated peaks,[2] the question of the properties of the states responsible for these peaks has been the subject of considerable speculation. From the absence of the peaks in π^+-p cross section,[3] it may be concluded that both states have isotopic spin $t = 1/2$. On the basis of the pion photoproduction measurements, Wilson suggested that the peak at 600 Mev corresponds to an excited state of the nucleon characterized by the angular momentum 3/2.[4] The 900-Mev level apparently corresponds to the $t = 1/2$, $J \geq 5/2$ excited state originally postulated by Cool et al.[2] but not resolved by them from the $t = 1/2$, $J = 3/2$ peak. However, the assignment of pion orbital angular momentum for both of these levels is ambigious: The 600-Mev level could be either $P_{3/2}^{1/2}$ or $D_{3/2}^{1/2}$,[5] while the higher one could be $D_{5/2}^{1/2}$, or $F_{5/2}^{3/2}$, or have $J \geq 5/2$. The cross-section data are shown in Fig. 1, in which are plotted the results of recent measurements on π^--p and π^+-p cross sections.

Information on the parity of the 600-Mev level comes from measurements of the polarization of the recoil protons in the reaction $\gamma + p \rightarrow p + \pi^0$. Stein,[7] confirmed by Connolly and Weill,[8] presents strong evidence that the parity of the 600-Mev level is opposite to that of the 300-Mev level (well known to be $P_{3/2}^{3/2}$), thereby identifying the 600-Mev level as $D_{3/2}^{1/2}$. However

interpretation of the measurements by Stein is not completely unambiguous, and the possibility still remains that the level may be $P_{3/2}^{1/2}$. The interpretation of the 900-Mev level is still more uncertain; in the absence of definite evidence (either pro or con) we adopt the prevailing hypothesis that this level may be $F_{5/2}^{1/2}$.[9]

If the nature of one of the levels were established, the different possible interpretations of the other could be checked by observation on the angular distribution of pions elastically scattered in the energy region in which the two levels interfere. This possibility is illustrated by the curves in Fig. 2, in which we show the angular distributions which would result from pure resonant scattering (Sec. III-B) under the two assumptions discussed above. When the diffraction-scattering contribution is added to these curves, it will completely dominate the scattering in the forward hemisphere. Only the angular distribution of π mesons in the backward hemisphere will be relatively unaffected by the diffraction scattering, and thus useful for making a clear distinction between the two hypotheses. In making this comparison, it does not seem necessary to know the absolute differential cross section but only the relative values (the shape) between 90 deg and 180 deg (c.m.). Since the backward pion angles correspond to forward angles of the recoil protons, an alternative approach is to measure the proton angular distribution in the forward hemisphere.

II. EXPERIMENTAL METHOD

A. Use of Nuclear Emulsions at Low Temperatures

The most accurate proton angular distribution measurements at low energies have been performed with nuclear emulsions. However, comparable accuracy has in general not been achieved in experiments at high energies, owing mainly to the very high general background at accelerators and the low intensity of the investigated beams; hence, the nuclear emulsion--an instrument incapable of time discrimination--has been used mainly as a qualitative tool. But the measurement of grain density allows for momentum determination over a relatively wide range of proton momenta; this suggests that, with the help of the kinematics of the (two-body) proton-emitting reaction in question, one should be able to discriminate the relevant proton tracks from the general background by accepting only a certain grain count at a given angle of proton emission. With this idea in mind we have made a set of measurements[10] with nuclear emulsions, referred to both angular and time distributions of the background, at the Brookhaven Cosmotron (Fig. 4). We found (a) that the angular distribution of the background is nearly isotropic; (b) the intensity of the background is proportional to the time of exposure, almost independent of the fluctuations of the machine-beam intensity; and (c) it is peaked at the ionization minimum but has a broad velocity distribution. From these studies we concluded that emulsions could be used as an angular-distribution and polarization detector in reactions such as π-p scattering, provided that the true track-to-background ratio could be increased by a factor of 10 to 100 over its normal value, thus allowing short exposures. This could be achieved either by increasing the π-beam intensity by the same factor--an unrealistic objective at the time

we were planning out experiment—or by placing the emulsions so close to the target—into the liquid hydrogen or in between it and the liquid nitrogen cooling agent—that the same factor is gained in the solid angle.

The behavior of emulsions at low temperatures has been studied by Waniek et al.[11] Their results indicated that large variations of the emulsion sensitivity are expected in the temperature region between liquid nitrogen and He; e.g., the liquid nitrogen sensitivity was reported to be about 75% of the 20 °C sensitivity, while at the temperature of liquid He it returned to 88% of the value at 20 °C. Since such variations, if real, would make any energy measurement based on the grain count unreliable, we decided to remeasure the emulsion sensitivity in the temperature region from 22 to 90 °K, with no special precautions taken for accuracy, but only to see if the sudden drops of sensitivity occurred anywhere in this temperature region. The temperature was measured with a copper-Constantan thermocouple; linearity of emf vs temperature was assumed between the boiling points of hydrogen and nitrogen. For none of the 30 G.5 pellicles did the grain count of the minumum-ionizing particles drop below 85% of the sensitivity at 20 °C; most plates showed 87% of the grain count at 20 °C. Typical grain-count values obtained are plotted in Fig. 3, together with the measurements by other authors. We did not find any sensitivity drops larger than those shown in the figure, in the emulsions used later in the actual experiment. However, since it is possible that sensitivity varies from batch to batch, and depends on the warming-up and the development procedure as well, we do not claim any quantitative accuracy for the results shown in Fig. 3.[12] Nevertheless, we conclude that

emulsions can be used in grain-count measurements between 22 °K and 90 °K. This has enabled us to subtend a solid angle about 50 times as large in the experiments with liquid H_2 as target, as would have been possible if we had had to place the emulsions outside the target.

B. Experimental Arrangement and Procedure

Figure 4 shows the beam geometry and the target-detector array at the Brookhaven Cosmotron. Negative π mesons, produced in an internal copper target, passed through a pair of strong-focusing magnets and a deflecting magnet. The median pion energy was 925±50 Mev; but taking into account the large energy spread and the shape of the resonance peak (Fig. 1), our "effective" pion energy was 892 Mev.

The target was placed behind a 12-ft Cosmotron shield in a concrete "house" with a 6-ft-thick wall and with a 1.5-ft steel roof. In a previous run[10] with a dummy target this shielding was found sufficient to reduce the background to 10% of its intensity without the house. The standard liquid hydrogen target used, with liquid nitrogen as a cooling agent, was originally designed by Lindenbaum. In order to avoid uncertainties due to the presence of material between the liquid hydrogen and the emulsions, we eliminated the usual metallic container (bronze foil), and poured the hydrogen straight into the Styrofoam container. The liquid hydrogen volume was 20×4×1.5 inches. The emulsions were placed in long slots in the Styrofoam walls, both left and right of the beam center, 1/2 in. from the liquid. Two such identical target assemblies were used alternately, with a number of spare Styrofoam containers. (The relatively thin Stryofoam walls between H_2 and the emulsions were likely to break owing to low-temperature stresses; two

such breaks actually occurred during the experiment. The temperature at the center of the batch of pellicles was about 35 °K. The plates (3×5 in.) in one position (forward) covered an angular range from 5 to 80 deg (12 to 164 c.m.), while the other (middle of the Styrofoam container) covered the region from 15 to 90 deg (35 to 180 deg c.m.). Two Victoreen ionization chambers were placed on each side, 2.5 in. from the beam center, against the target box, to monitor the radiation received by the emulsions. The ratio of the irradiation inside the target to the Victoreen reading outside the chamber was determined prior to the main run. The Victoreen readings were taken every 15 minutes during the exposures. A maximum irradiation dose of 25 mr to the plates was allowed.

A π-meson counter telescope was used to monitor the pion beam behind the target. An average intensity of about 10^5 π/cm^2 per 10^{11} primary protons was obtained during each run. The π beam was collimated to 3×3 in. The lateral intensity distribution, measured by the counter telescope, is shown in Fig. 5. The angular spread of the beam was estimated to be ± 3/4 deg.

We made four exposures with the π^- beam. In each of the four exposures an integrated flux of 3×10^8 π mesons was incident on the target in about 3 to 4 hours. The exposures were: (a) target completely empty; (b) nitrogen in the cooling system, hydrogen container empty; (c) and (d) actual runs with liquid hydrogen. The emulsions were brought to room temperature slowly and developed by a standard technique. The minimum grain count was determined from observing the π-μ-e decays.

The true-to-background ratio was determined to be 26:1 by counting the number of tracks per unit area of the 600 pellicles in runs (c) and (d) and comparing it with the same number from run (b). Typical numbers obtained at three different positions from the beam center are shown in Fig. 6.

C. Analysis of the Plates

The front region of each pellicle was scanned parallel to the front edge, from the middle of the pellicle outwards. The grain count and the direction angle of every track were measured. A 330-μ field of view was used to measure the angle; a magnification about two times as large was used to measure the grain count. The resulting distribution was plotted on a diagram of grain count g vs angle Θ, in which each track was represented by a dot. A typical experimental distribution for three plates is shown in Fig. 7. The solid lines represent the upper and the lower limits to the acceptable grain count. The width is due mainly to fluctuations in the grain count for cool emulsions and the energy spread of the initial beam, but other factors (target and the emulsion thickness traversed) were taken into account as well.

D. Corrections and the Result

To the angular distribution of proton tracks, as obtained from each plot like the one in Fig. 7, two geometrical corrections were applied, (a) target geometry correction, and (b) detector geometry correction, so that the angular distribution at every angular interval is multiplied by the geometrical correction factor

$$\frac{L(\Theta)}{L(45\ \text{deg})}\ \frac{A(\Theta)}{A(45\ \text{deg})}\ \frac{d\Omega}{d\omega}\ , \qquad (1)$$

where $L(\vartheta)/L(45\ \text{deg})$ and $A(\vartheta)/A(45\ \text{deg})$ are normalized target length and detector area respectively, and $d\Omega/d\omega$ is the conversion from lab to c.m. solid angle.

Apart from the geometrical corrections (a) and (b), a correction (c) was first made for total background due to both the inelastic processes in $\pi^- + p$ interaction and the general background. The number of dots per unit area was determined in that part of the g-ϑ diagram adjacent to the region of acceptable grain counts. We assumed that this gave also the approximate number of background particles in the region of the acceptable grain count, and subtracted it from the number obtained in each angular interval. This amounted to a correction of 2% to 8%, depending on the angular interval From the known data[13] on the cross section, and angular and momentum distributions of the inelastic process at 1 Bev, we estimated the expected background and found it to be in rough agreement with the observed background.

At small angles, less than 8 deg in the laboratory system, the proton tracks cannot be easily discriminated from those of π mesons. The ratio of specific ionizations is 1.06 to 1.1, and it rises rapidly with increase of the angle. Thus the point at $\cos\vartheta = -0.9$ is less reliable than the other points.

In all, about 1,600 tracks were measured. After all the corrections were applied to the observed distribution, the points were plotted against $\cos\vartheta_\pi$ the pion scattering angle in the center-of-mass system shown in Figs. 8 and 9. Typical numbers of

protons are given next to some of the points in Fig. 8. About 7/10 of the indicated errors are statistical in origin. The rest arise from uncertainty in normalizing our points to the absolute values of the differential cross section.

III. INTERPRETATION

A. Comparison with the Results of Erwin and Kopp

In Fig. 8, our results are compared with those of Erwin and Kopp,[14] who observed elastic π^--p scatterings in a hydrogen bubble chamber. The main difference between their data and ours is in the angular dependence in the region of $\cos \Theta_\pi \approx -0.5$.

This difference, although not far outside the statistical accuracy of their results and ours, serves to emphasize the difficulty of drawing firm conclusions, even of a qualitative nature, on the implications of such observations. Thus Erwin and Kopp had concluded, on the basis of the curves shown in Fig. 8, that the cross section at 950 Mev contains little "spin-flip" scattering, a conclusion which could not be drawn from a comparison of the same curves with our data.

The three curves drawn in Fig. 8 were computed on the following basis:

The curve labeled P_ℓ assumes pure spin-independent scattering (see Appendix I); it is a least-squares fit of the data of Erwin and Kopp to the formula

$$\frac{d\sigma}{d\Omega} = \lambda^2 \left| \sum_{\ell=0}^{4} (2\ell+1)\, a_\ell P_\ell \ (\cos \Theta) \right|^2 , \qquad (2)$$

with $a_\ell = e^{i\delta_\ell} \sin \delta_\ell$. The curves labeled P+D and D+F assume pure spin-flip scattering, i.e., $f(\theta)^\ell \approx 0$ (see Appendix I) with the main contributions to $g(\theta)$ arising from scattering in, respectively, the $P_{3/2}^{1/2}$ and $D_{3/2}^{1/2}$ state

and $D_{5/2}^{1/2}$ and $F_{5/2}^{1/2}$ states. Our data, in contrast with those of Erwin and Kopp, favor their D-F spin-flip curve.

However, as discussed in the following section, the analysis cannot be made on so simple a basis. Scattering in two resonant states which would lead to appreciable spin-flip, would also have an appreciable influence on the non-spin-flip scattering, in particular through interference with the nonresonant "diffraction" scattering which would arise from pion absorption and inelastic scattering, expected to be important at the energies of these experiments. It is also important to note that the rapid variation of phase shifts with incident pion energy, a characteristic of the resonant nature of the scattering, could lead to appreciable variation of the shape of the angular distribution with incident pion energy. Thus, the relatively small difference in the effective pion energy between our experiment and that of Erwin and Kopp might account for the difference, if real, in the observed angular distributions at large pion scattering angles. However, the data of the Bologna group,[15] obtained at a pion energy halfway between that of our experiment and the experiment of Erwin and Kopp, show features more similar to ours.

B. Phase-Shift Analysis

When the scattering depends on the total angular momentum ($j = l \pm 1/2$) as well as on l, the expression for the differential elastic scattering cross section becomes more complicated than Eq. (2):

$$\frac{d\sigma}{d\Omega} = \left| f(\theta) \right|^2 + \left| g(\theta) \right|^2 . \qquad (3)$$

Expressions for $f(\theta)$ and $g(\theta)$, the non-spin-flip and the spin-flip amplitudes, respectively, are given in terms of the phase shifts $\delta_{l, l \pm 1/2}$ in Appendix I.

In the case of a resonance in a given state (ℓ, j), the corresponding phase shift goes through 90 deg at the resonance energy.

The resonant phase shift may be obtained in terms of the parameters conventionally used to describe the resonance through the expression[16]

$$\eta_{res} = 1 - \frac{i\Gamma_{e\ell}}{(E-E_r)+i(\Gamma/2)} = e^{2i\delta} = a e^{2ia} , \qquad (4)$$

where E_r is the resonance energy, and $\Gamma_{e\ell}$ and Γ are the resonance widths for the elastic and total cross sections respectively. In general, for $\Gamma_{e\ell} < \Gamma$, δ is complex, and it is convenient to express the amplitude η in terms of the real constants a and a.

The resonance constants may be evaluated from the observed cross-section curves. In particular, at resonance

$$\sigma_{res}(E=E_r) = 4\pi \lambda_r^{\,2} \left(\frac{2j+1}{2}\right) \frac{\Gamma_{e\ell}}{\Gamma} . \qquad (5)$$

However, in the case of the observed pion-nucleon cross section curves, it is necessary first to separate the isotopic spin 1/2 and 3/2 components

$$\sigma(\pi^+ p) = (3/2) , \qquad (6a)$$

and

$$\sigma(\pi^- p) = \frac{2}{3}\,\sigma(1/2) + \frac{1}{3}\,\sigma\left(\frac{3}{2}\right) , \qquad (6b)$$

and also to subtract the background of nonresonant scattering before the resonant cross sections are obtained. Since there is a certain arbitrariness in this subtraction procedure, there is some ambiguity in the resonance parameters obtained by this procedure, especially in the energy region of interest to us.

1. Simple interpretation

A number of investigators have attempted to obtain the resonance parameters for the 600- and 900-Mev resonances by the procedure outlined ab. We have used the following values of the resonant phase shifts[17] evaluated a. t'. pion energy 900 Mev:

$a_{3/2} = 0.9, \quad \alpha_{3/2} = 161.2$ deg; (7a)

$a_{5/2} = 0.7, \quad \alpha_{5/2} = 90$ deg. (7b)

We have then evaluated the differential scattering cross section under two assumptions:

(a) $D_{3/2} - F_{5/2}$ combination —

$a_{2,3/2} = a_{3/2}, \quad a_{3,5/2} = a_{5/2}$; (8a)

$\alpha_{2,3/2} = \alpha_{3/2}, \quad \alpha_{3,5/2} = \alpha_{5/2}$.

All the rest of the $\delta_{\ell,\ell\pm1/2}$ are equal to 0:

(b) $P_{3/2} - F_{5/2}$ combination—

$a_{1,3/2} = a_{3/2}, \quad a_{3,5/2} = a_{5/2}$; (8b)

$\alpha_{1,3/2} = \alpha_{3/2}, \quad \alpha_{3,5/2} = \alpha_{5/2}$

All the rest of the $\delta_{\ell,\ell\pm1/2}$ are equal to 0.

The resulting differential elastic scattering cross sections are plotted vs cos Θ (c.m.) in Fig. 2.

2. Resonant plus hard-sphere scattering

The above interpretation has neglected the elastic scattering in all states other than those of the assumed resonances. Clearly, a reasonable analysis must take into account the "potential" elastic scattering in all states, including those in which there is a resonance. In order to obtain some qualitative idea of the effects of such potential scattering, we have computed the differential scattering cross section according to a crude (and admittedly inadequate) model, in which we have superimposed the diffraction scattering that would result from a hard sphere of radius

R = 1 fermi on the resonant scattering discussed in the preceding section. The (spin-independent) hard-sphere scattering phase shifts are obtained from the standard formula

$$\tan \delta_\ell = - \frac{j_\ell(k R)}{\eta_\ell(k R)} ,$$

are then combined with the resonant scattering phase shifts according to the prescription[16]

$$\eta_{\ell,j} = \eta_\ell \text{ (pot) } \eta\ell,j \text{ (res)} , \tag{10}$$

where

$$\eta_\ell(\text{pot}) = \exp[\, 2i\delta_\ell] , \tag{11}$$

and $\eta_{\ell,j}(\text{res})$ is given by Eq. (4). We have included only terms with $\ell \leq 3$, for which Eq. (9) gives $\delta_0 = -168$ deg, $\delta_1 = -97$ deg, $\delta_2 = -45$ deg, and $\delta_3 = -15$ deg. Using these values of δ_ℓ together with the resonance scattering phase shifts given in the preceding section, we obtain the cross sections plotted in Fig. 9.

IV. DISCUSSION

Our experimental results are compared with the computed cross-section curves in Fig. 9. The most distinctive feature of the computed curves, the strong maximum at $\cos \Theta \approx 0$, is clearly absent in the observations both by Erwin and Kopp (Fig. 8) and by us. However, we are not inclined to regard this as a singificant discrepancy, since this peak can be ascribed to our assumption of hard-sphere scattering, which is certainly not appropriate to the actual situation. A more reasonable model for the potential scattering would consider an absorbing sphere, with incomplete opacity (grey rather than black), possibly varying with position in the sphere, and probably

with a "fuzzy" boundary. Such a model is quite poorly approximated by our "hard" sphere; it would undoubtedly result in an appreciable reduction in the strength of the peak at approx 0 deg, as well as in diminution of the relative effects of the potential scattering at backward angles (the differences between our Fig. 3 and Fig. 9).

Nevertheless, a comparison of Figs. 3 and 9 serves to emphasize the possibility of relatively important effects of the nonresonant scattering on the angular distributions, even at the backward angles, and warns us of the necessity of taking such effects into account in interpreting such experiments.

Beyond this, we note especially from Fig. 3 that the angular distributions for resonant scattering are not markedly different in the two assumptions concerning the nature of the second (600-Mev) resonance.[18] Although our observations seem to weigh somewhat in favor of the $D_{3/2} - F_{3/2}$ combination, in confirmation of the conclusions of Stein,[7] we cannot presume to draw any firm conclusions from our data. Nor have we explored the consequences of other assumptions on the nature of the resonances (e.g., $P_{3/2} - G_{3/2}$), or the consequences of varying the absorption radius R or of introducing a finite transparency in an absorbing sphere. Also, we have tacitly assumed that the 1.35-Bev level(s) has (have) no influence on the angular distribution at 0.9 Bev.

We believe that some of the ambiguity of our conclusions could be resolved by measurements of the polarization of the elastically scattered recoil protons. Although it was not possible to obtain such a measurement in our experiment, owing to the high density of the tracks in our plates, we believe that using nuclear emulsions in conditions similar to those employed by us (but with only 1/3 or 1/4 of the number of protons per mm^2), will allow this type of measurement when using our result on polarization analysis by scattering in emulsions and an along-the-track method of scanning.

ACKNOWLEDGMENTS

We are indebted to Dr. L. O. Salant for invaluable aid in the conception, preparation, and execution of the exposures to the pion beam, to Dr. S. Lindenbaum, Dr. D. Hill, and H. Burrows for their help in measuring the π-beam intensity; and to the Brookhaven Cosmotron group and MIT scanning group for their cooperation.

Appendix I

The scattering amplitudes of Eq. (3) are given by the following expressions:

(Non-spin-flip)

$$f(\theta) = \frac{1}{2ik} \sum P_\ell (\cos\theta) \left[(\ell+1)(\eta_{\ell,\ell+1/2} - 1) + \ell (\eta_{\ell,\ell-1/2} - 1) \right];$$

(Spin-flip)

$$g(\theta,\phi) = \frac{1}{2ik} \sum Y_\ell^1 (\theta\phi) \sqrt{\frac{4\pi\ell(\ell+1)}{2\ell+1}} \left[\eta_{\ell,\ell+1/2} - \eta_{\ell,\ell-1/2} \right],$$

with

$$\eta_{\ell,j} = \exp[2i\delta_{\ell_j}] = a \exp[2i\alpha_{\ell_j}] \ .$$

For $a = 1$ (δ real)

$$1 - \eta = 2ie^{i\delta}\sin\delta \ . \qquad \text{(A}$$

Furthermore, for spin-independent scattering $\delta_{\ell,\ell+1/2} = \delta_{\ell,\ell-1/2}$, and Eq. (A1) reduces to Eq. (2), while $g(\theta,\phi) = 0$.

Finally, in the case of absorption $a < 1$ it is convenient to write

$$1 - \eta = (1 - a\,e^{2i\alpha}) \equiv b\,(1 - e^{2i\beta}) \ . \qquad \text{(}$$

Equating the real and imaginary parts gives

$$\tan\beta = \frac{1 - a + 2a\sin^2\alpha}{a\sin 2\alpha} \ ,$$

and

$$b = \frac{a\sin 2\alpha}{\sin 2\beta} \ .$$

The use of the form of $(1 - \eta)$ given in (A5) enables us to use all of the formulae conventionally developed for pure elastic scattering, with one simple substitution:

$$\sin \delta_{\ell,j} \rightarrow b \sin \beta_{\ell,j} \ , \tag{A8a}$$

$$\cos (\delta_{\ell,j} - \delta_{\ell',j'}) \rightarrow \cos (\beta_{\ell,j} - \beta_{\ell',j'}) \ . \tag{A8b}$$

Appendix II

Using Eqs. (A1-2) with terms including $\ell \leqslant 3$, the differential elastic scattering cross section may be expanded in a series of Legendre Polynomials

$$k^2 \frac{d\sigma}{d\Omega} = A P_0 + B P_1 + \cdots + G P_\ell(\cos\theta) \ . \tag{A9}$$

The coefficients A-G are given by sums of the form (Q representing, successively, A-G)

$$Q = \sum_{i} \sum_{\leqslant j} Q_{ij} b_i b_j \sin \beta_i \sin \beta_j \cos (\beta_i - \beta_j) \ , \tag{A10}$$

with the Q_{ij} as given in Tables I-VII below. For example, from Table II

$$\begin{aligned} B = {} & 2 b_{0,1/2} b_{1,1/2} \sin \beta_{0,1/2} \sin \beta_{1,1/2} \cos (\beta_{0,1/2} - \beta_{1,1/2}) \\ & + 4 b_{0,1/2} b_{1,3/2} \sin \beta_{0,1/2} \sin \beta_{1,3/2} \cos (\beta_{0,1/2} - \beta_{1,3/2}) \\ & + \cdots \cdots \cdots \cdots \\ & + \frac{72}{7} b_{2,5/2} b_{3,7/2} \sin \beta_{2,5/2} \sin \beta_{3,7/2} \cos (\beta_{2,5/2} - \beta_{3,7/2}) \ . \end{aligned}$$

All terms not included in the tables[20] have value 0.

Table I. A_{ij} coefficients in P_0

i	j	A_{ij}
$S_{1/2}$	$S_{1/2}$	1
$P_{1/2}$	$P_{1/2}$	1
$P_{3/2}$	$P_{3/2}$	2
$D_{3/2}$	$D_{3/2}$	2
$D_{5/2}$	$D_{5/2}$	3
$F_{5/2}$	$F_{5/2}$	3
$F_{7/2}$	$F_{7/2}$	4

Table II. B_{ij} coefficients in P_1

i	j	B_{ij}
$S_{1/2}$	$P_{1/2}$	2
$S_{1/2}$	$P_{3/2}$	4
$P_{1/2}$	$D_{3/2}$	4
$P_{3/2}$	$D_{3/2}$	4/5
$P_{3/2}$	$D_{5/2}$	36/5
$D_{3/2}$	$F_{5/2}$	36/5
$D_{5/2}$	$F_{5/2}$	18/35
$D_{5/2}$	$F_{7/2}$	72/7

Table III. C_{ij} coefficients in P_2

i	j	C_{ij}
$S_{1/2}$	$D_{3/2}$	4
$S_{1/2}$	$D_{5/2}$	6
$P_{1/2}$	$P_{3/2}$	4
$P_{1/2}$	$F_{5/2}$	6
$P_{3/2}$	$P_{3/2}$	2
$P_{3/2}$	$F_{5/2}$	12/7
$P_{3/2}$	$F_{7/2}$	72/7
$D_{3/2}$	$D_{3/2}$	2
$D_{3/2}$	$D_{5/2}$	12/7
$D_{5/2}$	$D_{5/2}$	24/7
$F_{5/2}$	$F_{5/2}$	24/7
$F_{5/2}$	$F_{7/2}$	8/7
$F_{7/2}$	$F_{7/2}$	100/21

Table IV. D_{ij} coefficients in P_3

i	j	D_{ij}
$S_{1/2}$	$F_{5/2}$	6
$S_{1/2}$	$F_{7/2}$	8
$P_{1/2}$	$D_{5/2}$	6
$P_{3/2}$	$D_{3/2}$	36/5
$P_{3/2}$	$D_{5/2}$	24/5
$D_{3/2}$	$F_{5/2}$	24/5
$D_{3/2}$	$F_{7/2}$	8/3
$D_{5/2}$	$F_{5/2}$	16/5
$D_{5/2}$	$F_{7/2}$	8

Table V. E_{ij} coefficients in P_4

i	j	E_{ij}
$P_{1/2}$	$F_{7/2}$	8
$P_{3/2}$	$F_{5/2}$	72/7
$P_{3/2}$	$F_{7/2}$	40/7
$D_{3/2}$	$D_{5/2}$	72/7
$D_{5/2}$	$D_{5/2}$	18/7
$F_{5/2}$	$F_{5/2}$	18/7
$F_{5/2}$	$F_{7/2}$	360/77
$F_{7/2}$	$F_{7/2}$	324/77

Table VI. F_{ij} coefficients in P_5

i	j	F_{ij}
$D_{3/2}$	$F_{7/2}$	40/3
$D_{5/2}$	$F_{5/2}$	100/7
$D_{5/2}$	$F_{7/2}$	40/7

Table VII. G_{ij} coefficients in P_6

i	j	G_{ij}
$F_{5/2}$	$F_{7/2}$	200/11
$F_{7/2}$	$F_{7/2}$	100/33

FOOTNOTES AND REFERENCES

*Work done under the auspices of the U. S. Atomic Energy Commission.

†Now at Lawrence Radiation Laboratory, Berkeley, California.

‡On leave of absence at CERN, Geneva.

1. D. H. Frisch, D. M. Ritson, H. C. Burrows, D. O. Caldwell, D. O. Hill, R. A. Schluter, and M. A. Waklig, Phys. Rev. Letters 2, 119 (1959).
2. R. Cool, O. Piccioni, and D. Clark, Phys. Rev. 103, 1082 (1956).
3. See, however, P. Carruthers and H. A. Bethe, Phys. Rev. Letters 4, 536 (1960).
4. Robert R. Wilson, Phys. Rev. 110, 1212 (1958).
5. In this notation the superscript stands for I-spin t, and the subscript for total angular momentum J.
6. T. J. Devlin, B. C. Barish, W. H. Hess, V. Perez-Mendez, and J. Solomon, Phys. Rev. Letters 4, 242 (1960).
7. P. C. Stein, Phys. Rev. Letters 2, 473 (1959).
8. P. L. Connolly and R. Weill, Bull. Am. Phys. Soc. 4, 23 (1959).
9. G. Bernardini, Summary Report at the Kiev Conference, 1959 (unpublished).
10. B. T. Feld and B. C. Maglić, Massachusetts Institute of Technology, LNS Progress Report, August 31, 1956, p. 69.
11. R. W. Waniek, Bull. Am. Phys. Soc. 1, 219 (1956).
12. We used Ilford G.5, 400 and 600 μ, serial Nos. 236, 9779, and 9850.
13. I. Derado and N. Schmitz, Phys. Rev. 118, 309 (1960).
14. A. R. Erwin, Jr. and J. K. Kopp, Phys. Rev. 109, 1364 (1958).
15. V. Bergia, Borelli, Lavatelli, Manguzzi, Rausi, P. Woloschek, V. Zoboli, Barutti, Chersovani, and Tosi, Annual International Conference on High-Energy Nuclear Physics (CERN, Geneva, 1958), p. 67.

16. J. M. Blatt and V. F. Weisskopf, Theoretical Nuclear Physics (John Wi... and Sons, 1952), Chap. 8.

17. We are beholden to W. M. Layson at CERN for the results of his analysis of the pion-nucleon resonance parameters.

18. This conclusion is somewhat at variance with predictions that disregard the absorption in the resonances (i.e., that take a = 1). This again emphasizes the necessity of further observations to remove ambiguit... from the interpretation of the experimental data.

19. B. T. Feld and B. C. Maglić, Phys. Rev. Letters 1, 375 (1958).

20. A corresponding expansion in a series of cos n θ has been tabulated i... John I. Shonle, Differential Elastic Pion-Proton Scattering at 600, 650, and 750 Mev (Ph. D. Thesis), Lawrence Radiation Labo... Report UCRL-9362, August 12, 1960 (unpublished).

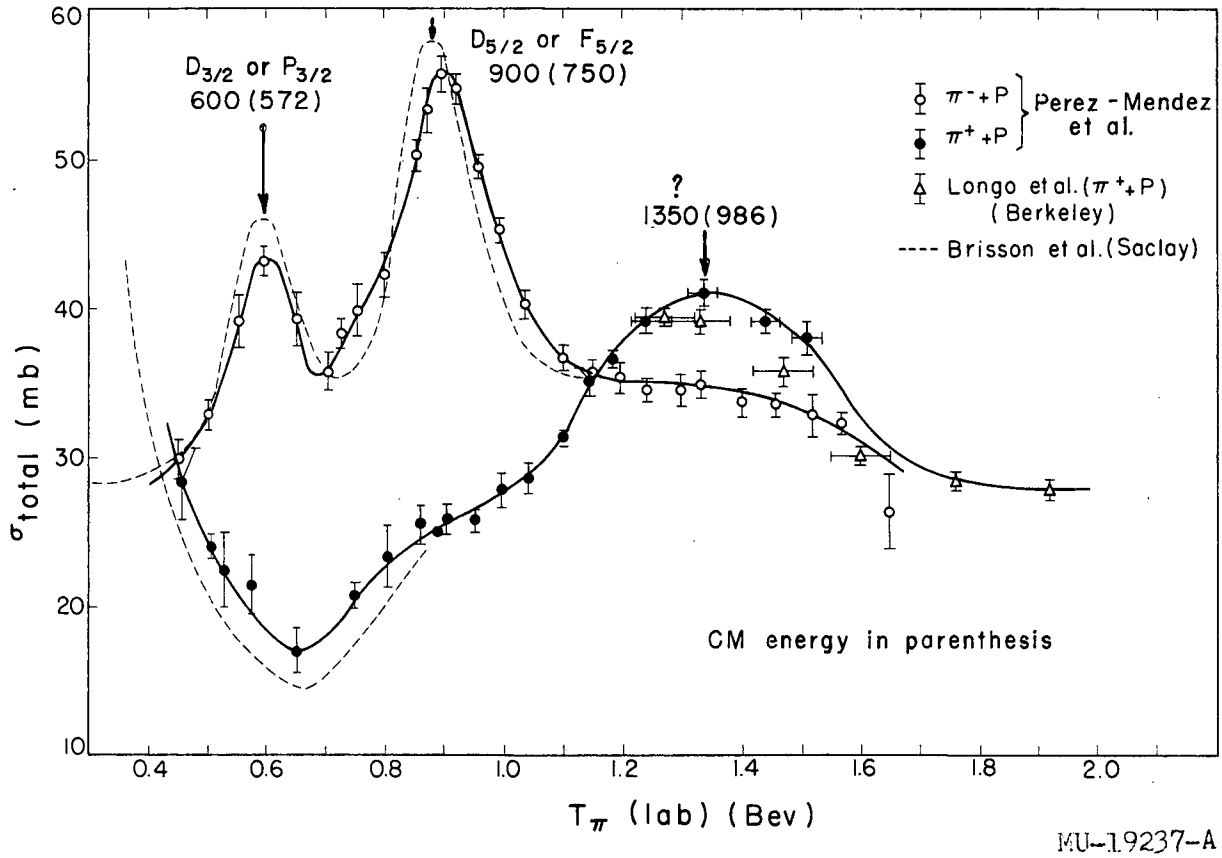

Fig. 1. Total cross section for π^- + p and π^+ + p scattering vs pion kinetic energy in the laboratory system. For all references see Ref. 4.

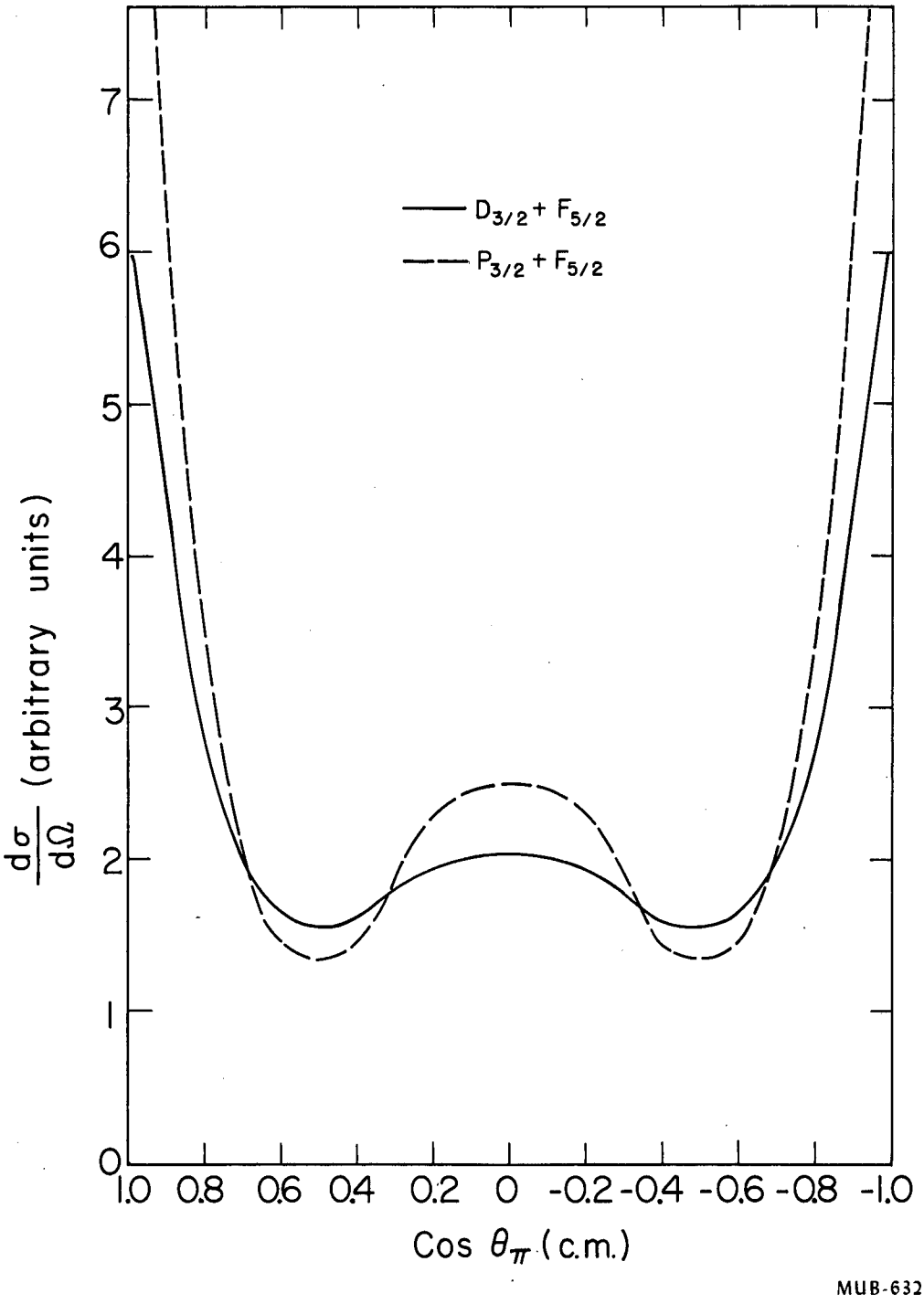

Fig. 2. Differential cross section for pure spin-flip scattering, as calculated in Sec. III-B.

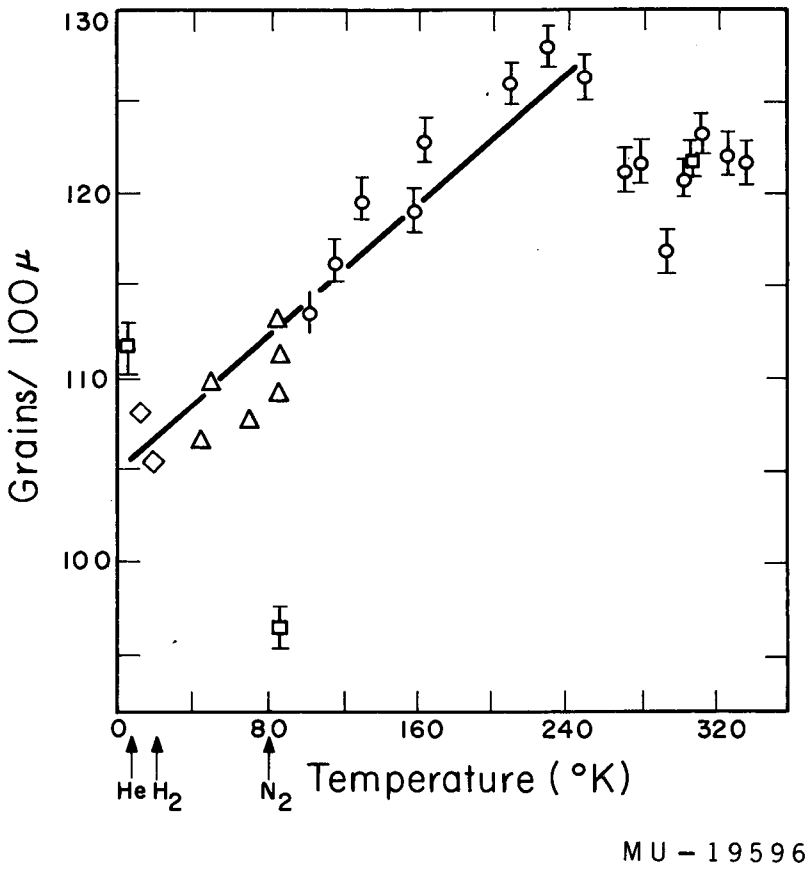

Fig. 3. Relative sensitivity of nuclear emulsions as a function of temperature. The triangles are our points; all other points are those of Waniek (Ref. 11).

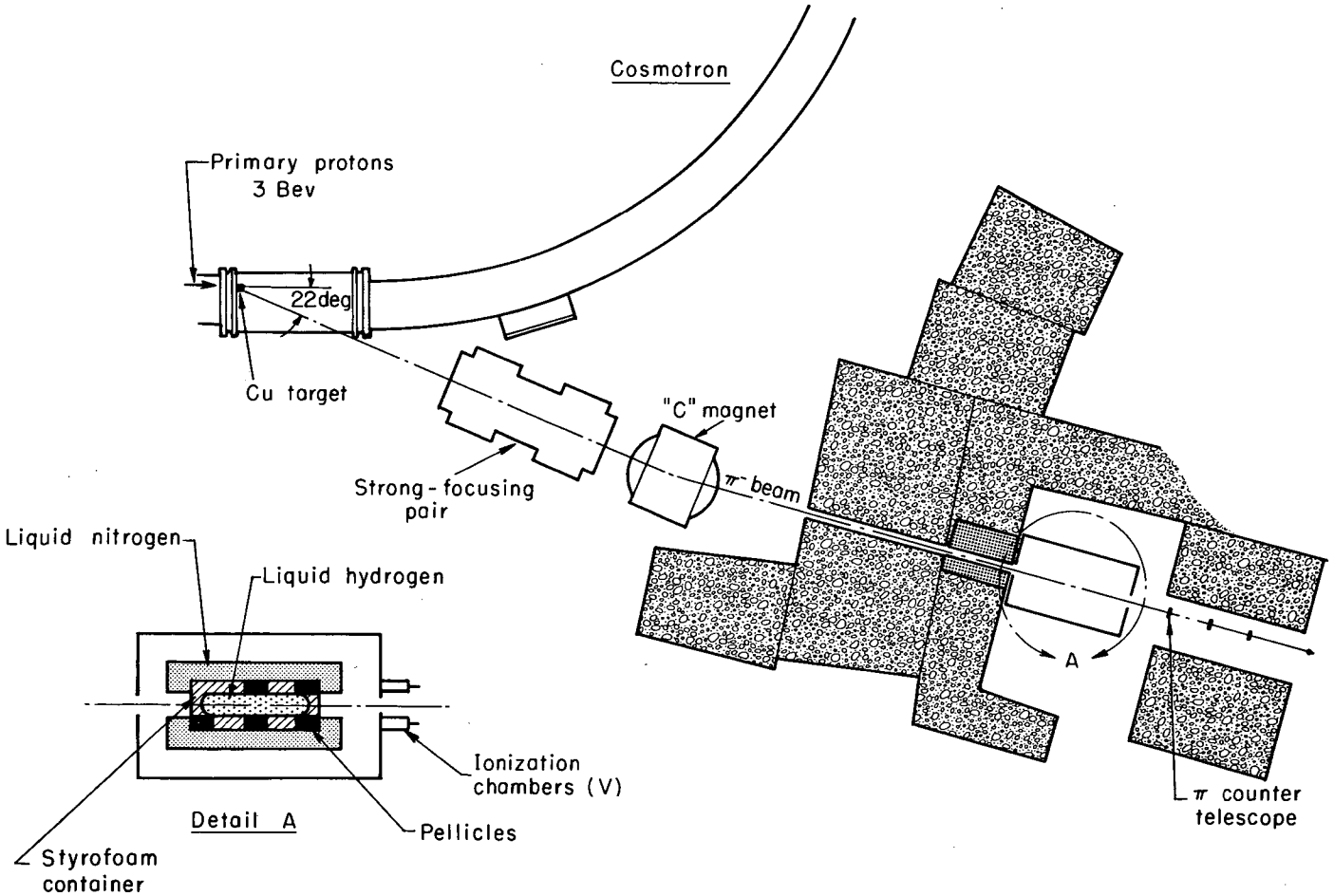

Fig. 4. Experimental arrangement.

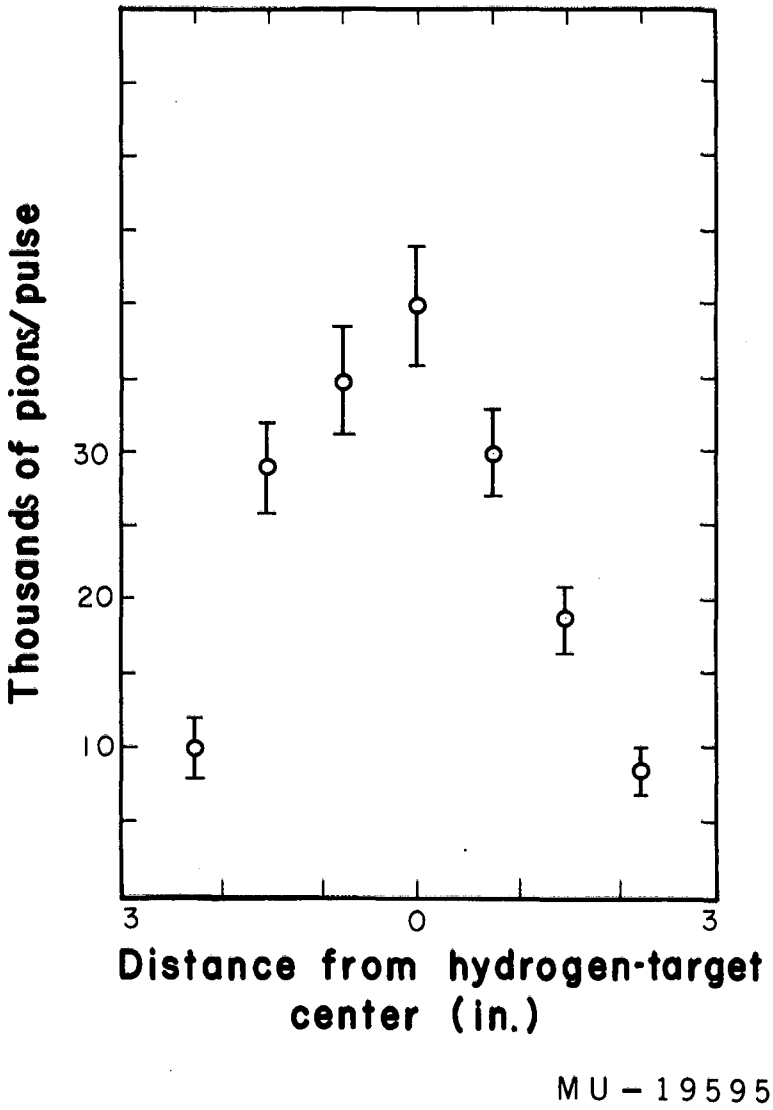

Fig. 5. Lateral intensity distribution of the π mesons in the beam, measured by counter telescope.

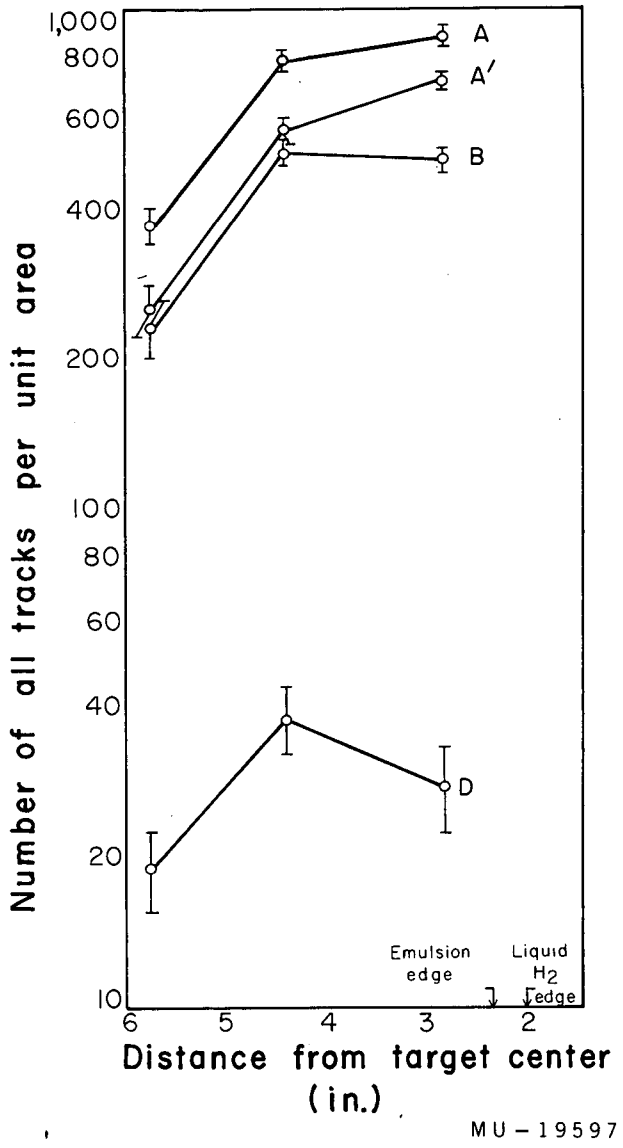

Fig. 6. Number of tracks per unit area of 600-μ emulsion obtained during a run, (b) without, and (c) and (d) with, liquid hydrogen in the target container.

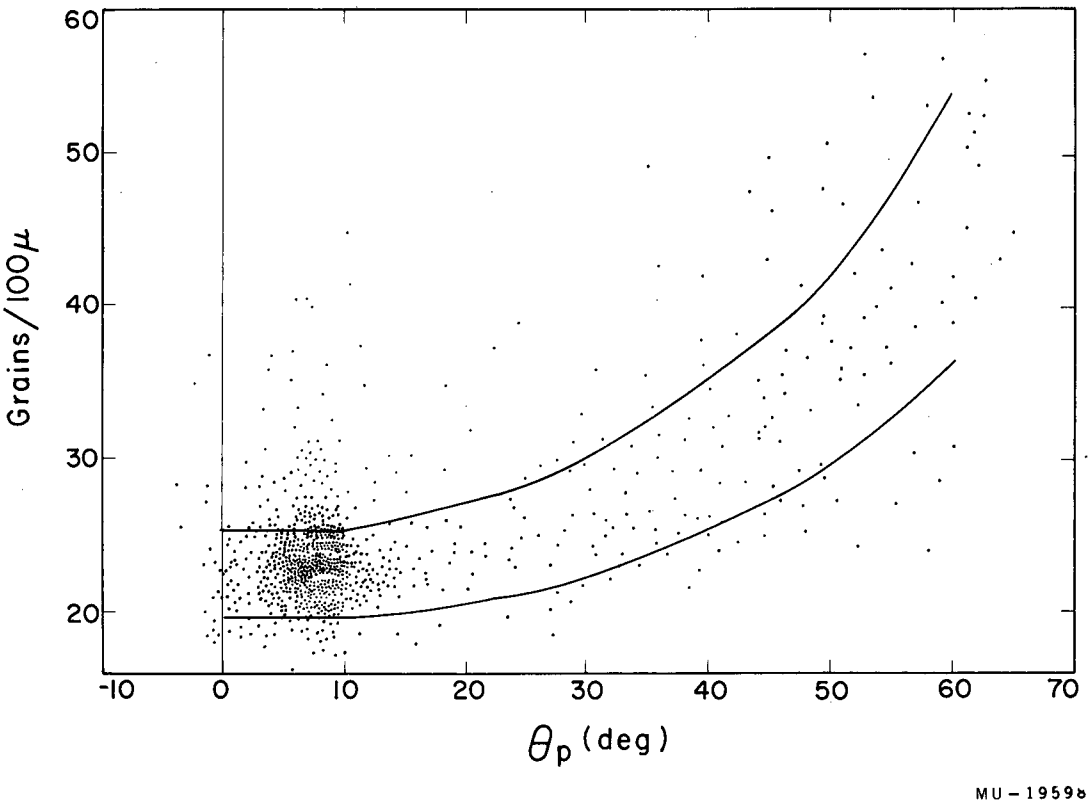

Fig. 7. Direction angle vs grain count distribution; typical experimental data obtained from four pellicles.

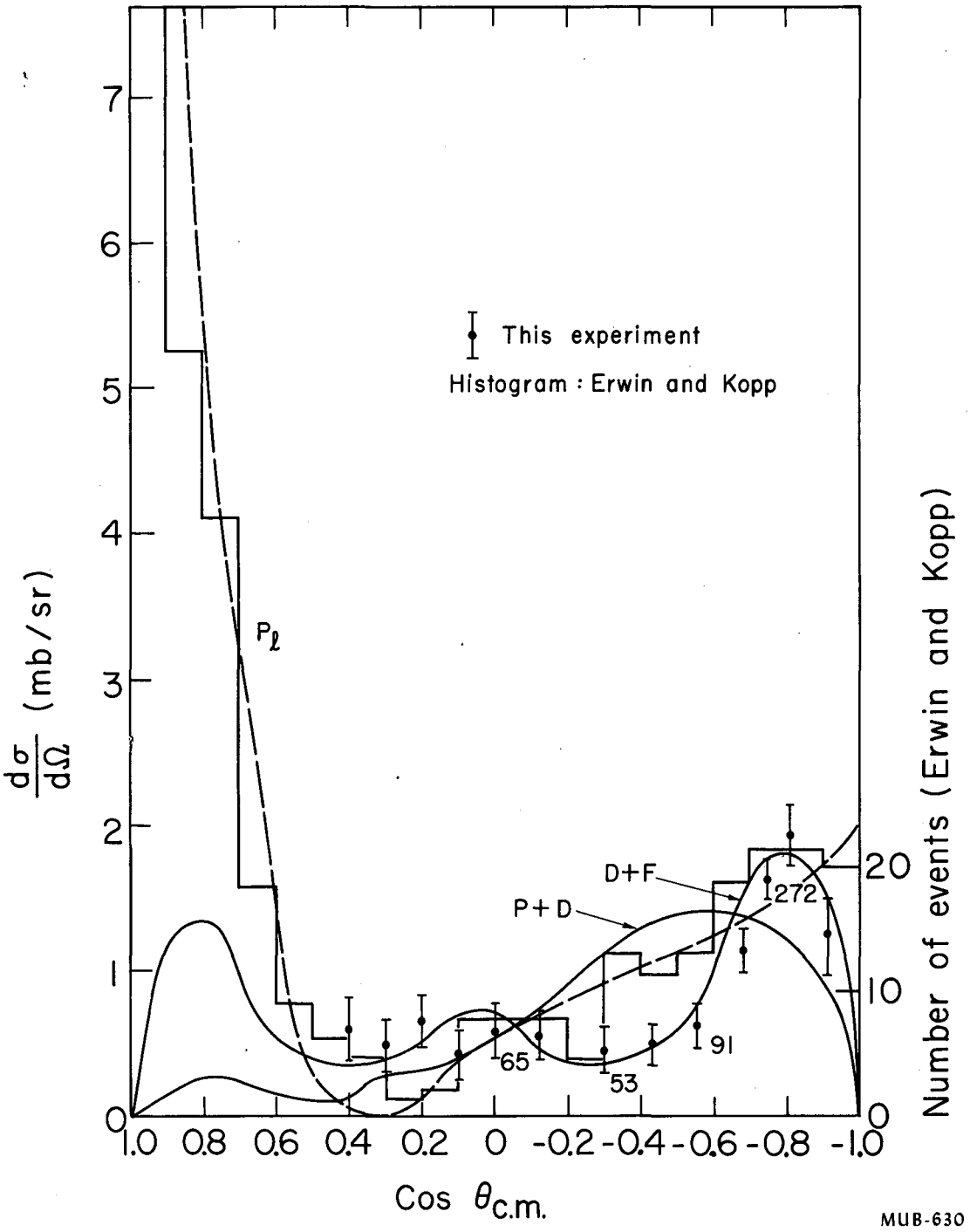

Fig. 8. Differential cross section for $\pi^- + p$ scattering vs cos θ, where θ is the pion scattering angle in the center-of-mass system. Typical numbers of protons are given next to some of our points. The data on Erwin and Kopp (histogram) are obtained at 950-Mev pion energy. The curves are discussed in Sec. III-A.

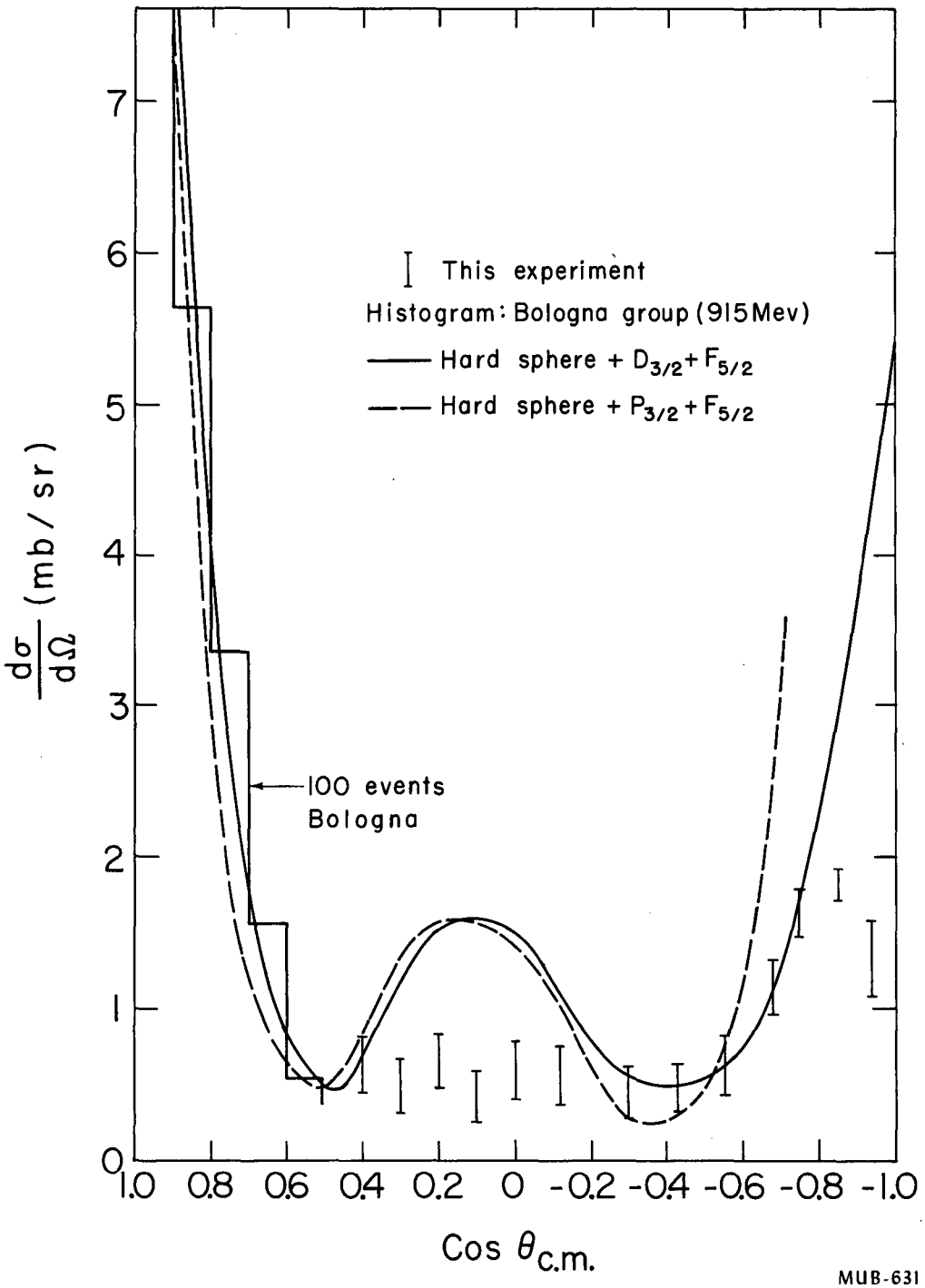

Fig. 9. Differential cross section for π^- + p scattering vs cos θ, where θ is the pion center-of-mass angle. The experimental points are the same as those in Fig. 8. The curves are calculated in Sec. III-B.